

# From few to many bosons inside the unitary window: a transition between universal to non-universal behavior

A. Kievsky,<sup>1</sup> A. Polls,<sup>2</sup> B. Juliá-Díaz,<sup>2</sup> N. K. Timofeyuk,<sup>3</sup> and M. Gattobigio<sup>4</sup>

<sup>1</sup>*Istituto Nazionale di Fisica Nucleare, Largo Pontecorvo 3, 56100 Pisa, Italy*

<sup>2</sup>*Departament de Física Quàntica i Astrofísica, Facultat de Física,  
Universitat de Barcelona, E-08028 Barcelona, Spain*

<sup>3</sup>*Department of Physics, University of Surrey, Guildford, Surrey GU2 7XH, United Kingdom*

<sup>4</sup>*Université Côte d'Azur, CNRS, Institut de Physique de Nice,  
1361 route des Lucioles, 06560 Valbonne, France*

Universal behaviour in few-bosons systems close to the unitary limit, where two bosons become unbound, has been intensively investigated in recent years both experimentally and theoretically. In this particular region, called the unitary window, details of the inter-particle interactions are not important and observables, such as binding energies, can be characterized by a few parameters. With an increasing number of particles the short-range repulsion, present in all atomic, molecular or nuclear interactions, gradually induces deviations from the universal behaviour. In the present letter we discuss for the first time a simple way of incorporating non-universal behaviour through one specific parameter which controls the smooth transition of the system from universal to non-universal regime. Using a system of  $N$  helium atoms as an example we calculate their ground state energies as trajectories within the unitary window and also show that the control parameters can be used to determine the energy per particle in homogeneous systems when  $N \rightarrow \infty$ .

**Introduction.** Close to the unitary limit, the physical behaviour and properties of few-body systems are driven and shaped by universality and this has far-reaching consequences for  $N$ -particle systems. At this limit a two-body system has a bound state at its decay threshold, with the two particles staying mostly outside the region of their interaction. The properties of this system are determined by one parameter, the two-body energy length  $a_B$ , defined from the two-body binding ( $a_B > 0$ ) or virtual ( $a_B < 0$ ) energy  $E_2 = \hbar^2/ma_B^2$  ( $m$  is the particle mass). In the limit of a zero-range interaction, the two-body scattering length  $a$  and the energy length are equal,  $a = a_B$ , and the two-body system shows a continuous scale invariance. For finite range interactions  $a \neq a_B$  and the difference  $r_B = a - a_B$ , called the finite-range parameter, defines the unitary window if the condition  $r_B/a_B \approx r_B/a \ll 1$  is satisfied.

The special nature of the unitary window shows up in a dramatic way in the energy spectrum of three-body systems, as shown by V. Efimov for the case of a zero-range attractive interaction [1, 2]. The system has a discrete scale invariance which is manifest at unitarity by the Efimov effect: an infinite tower of geometrically-distributed energy states with the neighbouring energies ratios of  $\approx 515$ . Intense experimental efforts, notably in the field of ultracold quantum gases [3–8], as well as theoretical studies [9, 10] have been dedicated to this subject, including larger systems [11–15] or those with different symmetries [16–18].

A large class of systems inside the unitary window is well described using a simple gaussian interaction,

$$V(r_{ij}) = V_0 e^{-r_{ij}^2/r_0^2} \quad (1)$$

with a variable strength  $V_0$  ( $r_{ij}$  is the interparticle dis-

tance) [14, 20]. In this way the universal behavior, exactly verified in the case of zero-range interactions, is extended to include finite-range corrections [21]. Finite range effects become more important when the interparticle distance inside the  $N$ -boson clusters gets sufficiently small so that the short-range physics starts to manifest explicitly in a non-universal way because of a different repulsive core in each particular system. This effect shows up smoothly with an increasing number of particles driving the system from a universal regime to a non-universal one.

In this letter we study the transition to non-universality in a two step analysis. First of all, we perform a gaussian characterization of the unitary window of the  $N$ -boson system by constructing trajectories in the energy plane ( $E_2, E_N$ ) using the interaction potential of Eq. (1). In this plane, any system can be represented by a point, called the physical point, determined when the  $E_2$  and  $E_N$  ground state energies are simultaneously reproduced by the gaussian parameters. In the case of ultracold atomic gases, tunable Feshbach resonances can be used to explore experimentally the unitary window [22]. It can be also explored theoretically by varying the interparticle potential. The movement of the system along the path determined by the gaussian form reveals its universal character.

The second step of our analysis uses the effective field theory (EFT) framework introduced to describe boson systems with large two-body scattering lengths [23, 24]. In this formalism the potential in Eq. (1) enters at leading order (LO); at the same order a three-body force is needed to counterbalance the dependence introduced by the gaussian range  $r_0$ . The strengths of the two- and three-body LO terms are determined by two control pa-

rameters,  $E_2$  and  $E_3$ . In a universal regime the energies  $E_N$ ,  $N > 3$ , are completely determined by the two control parameters, except for a residual range dependence [25]. We explore this dependence and show that the range of the three-body force, that could differ from the two-body range  $r_0$ , emerges as a non-universal scale parameter useful to describe the  $N$ -boson systems inside the window. Using helium systems as an example, by setting this parameter to describe  $E_4$  together with  $E_2$  and  $E_3$ , we show that energies per particle,  $E_N/N$ , as  $N \rightarrow \infty$  can be well reproduced.

**Gaussian characterization for  $N$  bosons.** The ground state energies of  $N = 2, 3, 4$  bosons along the unitary window, obtained using the gaussian interaction of Eq. (1), are represented in Fig. 1 through their binding momenta  $\kappa_N$ , defined from  $E_N = \hbar^2 \kappa_N^2 / m$ . They are plotted as functions of the inverse of  $a_B$  and all quantities are made dimensionless by being scaled by the gaussian range  $r_0$ . The figure relates few- and two-body energies in a unique way: gaussians with different ranges and strengths give results that always lie on the same curves. At unitarity the quantities  $\kappa_N^* r_0 = 0.4883$  and  $1.1847$ , for  $N = 3, 4$ , respectively, are the same for all gaussian interactions. These points are highlighted in the left panel of Fig. 1.

Real systems are located on the gaussian plot of Fig. 1 through the energy ratio  $E_N/E_2$ . As an example we discuss clusters of He atoms which are among a few physical systems naturally existing inside the unitary window. Early estimates of the two-body scattering length  $a \approx 180 a_0$  and the dimer energy  $E_2 \approx 1$  mK were given in [26]. Recently  $E_2 = 1.70 \pm 0.15$  mK was measured by Coulomb explosion [27]. Due to the relatively large experimental uncertainty in these values we plot results of theoretical calculations for these systems noticing that a few of them agree with the measured values. We consider two-, three- and four-body energies calculated in Ref. [28] for a variety of realistic He-He interactions shown in Table I. Using these results we calculate the ratios  $E_3/E_2$  and  $E_4/E_2$  and display the physical points, corresponding to the interactions listed in Table I, in the right panel of Fig. 1. A particular gaussian range  $r_0$  can be determined for each He-He potential from the corresponding axis values,  $r_0/a_B$  or  $r_0\kappa_N$ . Interestingly, the different  $r_0/a_B$  (or  $r_0\kappa_N$ ) axis values, associated with different He-He potentials, correspond to an almost unique value of  $r_0$  in each case of  $N$ :  $r_0^{(3)}$  for  $N = 3$  and  $r_0^{(4)}$  for  $N = 4$ , both shown in Table I.

The fact that all  $r_0$  values, determined by different realistic He-He potentials, are practically the same for a given  $N$  allow us to construct the following gaussian potentials

$$V^{(N)}(r_{ij}) = V_0^{(N)} e^{-r_{ij}^2/(r_0^{(N)})^2}, \quad \text{with } N = 3, 4. \quad (2)$$

We will call  $r_0^{(N)}$  the characteristic range. Choosing spe-

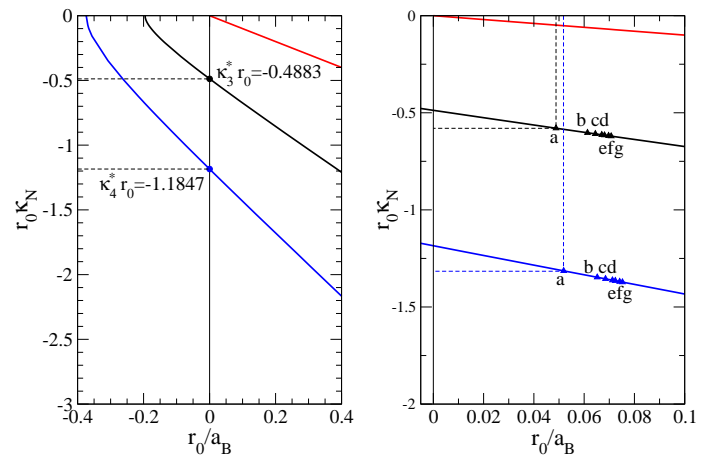


FIG. 1. Binding momentum in terms of the inverse of  $a_B$  for a gaussian potential, in units of the gaussian range  $r_0$ . The cases  $N = 2, 3, 4$  are shown by the red, black, and blue solid lines, respectively (left panel). Specific helium trimers and tetramers are located on the plot, see text for details. As an example, the dashed lines mark the location of the “a” point.

Potential	$E_2$	$E_3$	$E_4$	$r_0^{(3)}(a_0)$	$r_0^{(4)}(a_0)$
a: HFD-HE2[29]	0.8301	117.2	535.6	11.146	11.840
b: LM2M2[30]	1.3094	126.5	559.2	11.150	11.853
c: HFD-B3-FCH[31]	1.4475	129.0	566.1	11.148	11.853
d: CCSAPT[32]	1.5643	131.0	571.7	11.149	11.851
e: PCKLJS[33]	1.6154	131.8	573.9	11.148	11.852
f: HFD-B[34]	1.6921	133.1	577.3	11.149	11.854
g: SAPT96[35]	1.7443	134.0	580.0	11.147	11.850

TABLE I. Dimer, trimer and tetramer energies (in mK) for the indicated potential (the labels indicate the points on Fig. 1). Values (except for the HFD-HE2 potential) are from Ref. [28]. The last two columns show the  $N = 3, 4$  characteristic gaussian ranges.

cific  $V_0^{(3)}$  values, with the average range  $r_0^{(3)} = 11.147 a_0$ , the above potential can reproduce simultaneously the dimer and trimer energies of different realistic He-He potentials. Similarly, specific  $V_0^{(4)}$  choices can reproduce the dimer and tetramer energies. The potentials  $V^{(3)}$  and  $V^{(4)}$  can be thought of as low energy representations of the realistic interactions. We will call them characteristic gaussian potentials. Decreasing the gaussian strengths allows the unitary limit to be reached where the relations  $\kappa_3^* r_0^{(3)} = 0.4883$  and  $\kappa_4^* r_0^{(4)} = 1.1847$  can be used to calculate the values

$$E_3^* = 83.05 \pm 0.05 \text{ mK} \quad (3)$$

$$E_4^* = 433.0 \pm 0.5 \text{ mK}. \quad (4)$$

They should be compared to the values  $E_3^* \approx 84.0$  mK and  $E_4^* \approx 439.0$  mK obtained for the realistic potentials once their strength is varied to locate three- and four-

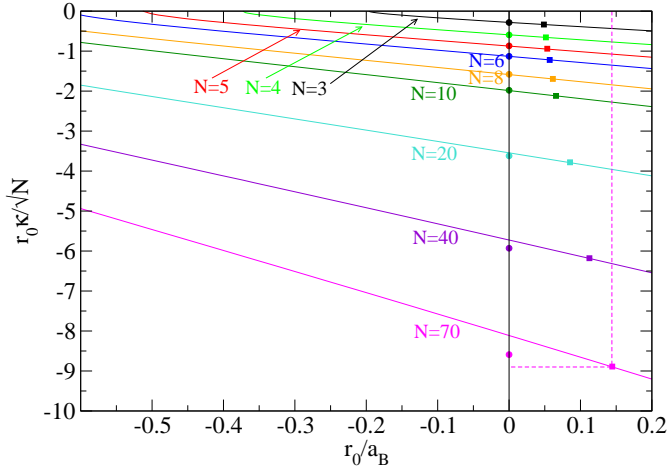


FIG. 2. The binding momentum per particle  $\kappa_N/\sqrt{N}$  in terms of the inverse of  $a_B$  for a gaussian interaction (in units of the gaussian range  $r_0$ ) and for selected number of particles. For each  $N$  value, the lines collect the results of every gaussian potential. The solid squares are the values of the HFD-HE2 potential, the position of each point determines the axis values  $r_0/a_B$  and  $r_0\kappa_N/\sqrt{N}$ , as shown by the dashed (magenta) line in the  $N = 70$  case, from which the characteristics range  $r_0^{(N)}$  can be determined. The solid circles at the unitary limit (vertical axis) show the values  $r_0^{(N)}\kappa_N^*/\sqrt{N}$  calculated using the HFD-HE2 potential at unitarity, i.e., when the potential is multiplied by the factor  $\lambda = 0.9792445$ .

body systems at the unitary limit [36]. The quality of the description is around 1% which is a remarkable result. The gaussian energy curves coincide with those obtained using reduced-depth realistic helium potentials. In other words, the characteristic gaussian potentials determine a path followed by the realistic systems all the way towards the unitarity where the  $r_0^{(N)}\kappa_N$  values do not depend on the choice of one specific He-He potential. This can be seen as an evidence for universal behaviour.

Next we use the gaussian potential of Eq. (1) to characterise the unitary window for larger number of particles  $N$ . Using the hyperspherical harmonic method [37, 38], we calculate the ground state energies for a selected range of  $N$  and depict the results in Fig. 2. The energies of the boson systems interacting with the realistic HFD-HE2 potential are shown in the same figure (solid squares). When this potential is multiplied by a factor  $\lambda$  to reach the unitarity limit it gives the results indicated by the solid circles. We can observe that at unitarity the energies  $E_N$  are on top of the gaussian trajectories until  $N = 10$ , suggesting strongly an independence of the interaction details, and, with small deviations, for  $10 < N \leq 20$ . Above  $N = 20$  noticeable differences are observed for  $N = 40$  and  $70$  as the short-range physics starts to play a role, resulting in a smooth transition from a universal to a non-universal regime.

**Soft gaussian potential.** We have shown above that systems with low values of  $N$  display universal behaviour in the unitary window. However, the description in terms of the characteristic range,  $r_0^{(N)}$ , deteriorates as  $N$  increases. To deeper analyse this transition we make use of the EFT framework for systems having a large value of the two-body scattering length. At LO of this theory [9, 23, 24] the potential consists of a two- plus a three-body term determined to reproduce the dimer and trimer energies. We use the following soft gaussian potential (SGP)

$$V = V_0 \sum_{i < j} e^{-r_{ij}^2/r_0^2} + W_0 \sum_{i < j < k} e^{-2\rho_{ijk}^2/\rho_0^2} \quad (5)$$

with  $\rho_{ijk}^2 = (2/3)(r_{ij}^2 + r_{jk}^2 + r_{ki}^2)$ . In the following we use the He-He potential HFD-HE2 as a reference potential to make a contact with a previous work [39], where saturation properties of helium drops were studied from a leading order description. For  $N = 2$  (with  $\hbar^2/m = 43.281307 \text{ K} a_0^2$ ), this potential gives a single bound state,  $E_2 = 0.83012 \text{ mK}$ , a scattering length  $a = 235.547 a_0$  and the finite-range parameter  $r_B = 7.208 a_0$ . For  $N = 3$  and  $N = 4$  the HFD-HE2 ground state energies are given in Table I, obtained using the correlated hyperspherical harmonic basis [40] and diffusion Monte Carlo method, respectively. They are in good agreement with the Green Function Monte Carlo results of Ref. [41]. Reducing the strength of the HFD-HE2 by the factor  $\lambda$ , we decrease the He-He energy down to zero. Then we obtain  $E_3 = 83.80 \text{ mK}$  and  $E_4 = 439.6 \text{ mK}$  in close agreement with the results of the other realistic potentials.

For a chosen pair of the two- and three-body gaussian ranges  $r_0$  and  $\rho_0$  we fix the SGP strengths  $V_0$  and  $W_0$  to reproduce the HFD-HE2 energies  $E_2$  and  $E_3$ . Then we use this SGP to calculate the tetramer energy  $E_4$ . In Fig. 3 the narrow (green) band shows  $E_4$  as a function of  $r_0$ . The band collects the results for different values of  $\rho_0$ , its lowest part is given by the lowest value of  $\rho_0$  considered,  $\rho_0 = 3 a_0$ , reducing further this value no increase of  $E_4$  is obtained. This means that for given values of  $r_0$  the possible values of  $E_4$  are limited and, more importantly, only a restricted range of  $r_0$  values is compatible with the energy value given by the reference realistic potential and indicated in Fig. 3 by the green horizontal line. In the figure the vertical line indicates the  $r_0$  value at which both,  $E_2$  and the two-body scattering length  $a$ , coincide with those of the reference potential HFD-HE2. At this particular value,  $a - a_B = r_B \approx 7.2 a_0$ , the best description of  $E_4$  is obtained. In Fig. 3 the largest value of  $r_0$  considered is equal to the characteristic range  $r_0^{(3)}$ , the one that describes the trimer energy in the simple two-body gaussian model of Eq.(2). At this value the three-body force is zero and higher  $r_0$  values lead to an attractive three-body force not considered in the present analysis. It should be noticed that in the region limited

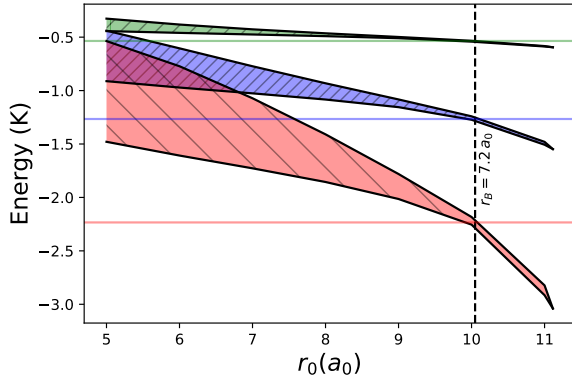


FIG. 3.  $E_4$  (green band),  $E_5$  (blue band) and  $E_6$  (orange band), as functions of the two-body range  $r_0$ , obtained with the three-body range,  $3 a_0 \leq \rho_0 \leq 11 a_0$ . The reference energies of the HFD-HE2 potential are given as horizontal lines. The vertical line indicates the reference  $r_B$  value. Notice that the dimer and trimer energies are always reproduced for all the SGP interactions considered.

by  $r_0^{(3)}$  and the vertical line the  $E_4$  band is very narrow indicating a low dependence on the three-body range.

Fig. 3 also shows the energy bands obtained for  $N = 5, 6$  systems. In general, they are broader than the one corresponding to the  $N = 4$  case. However, with the SGP parameters reproducing  $r_B$  at physical point the  $N = 5, 6$  bands become narrow and, more importantly, pass through the reference HFD-HE2 energies. A detailed analysis of the results indicates that the best, simultaneous, description of  $E_5$  and  $E_6$  is obtained when the two-body term of the SGP potential reproduces the finite range parameter  $r_B$  and when the three-body range  $\rho_0$  is fixed to optimize the description of the tetramer energy. The optimum set of these values is given in Table II with the corresponding values of  $E_4$ - $E_6$  and the HFD-HE2 reference energies, marked as “physical point”. In this point the SGP parameters coincide with those of Ref. [39]. A similar analysis at the unitary point produces the SGP parameters and results given in the right part of Table II.

Now we extend our analysis to heavier systems following a different strategy to the one that has already been used to study few-body systems close to the unitary limit at leading order of the EFT [15]. There, in order to reduce the residual range dependence of the observables, the  $N \leq 6$  binding energies have been studied as  $r_0 \rightarrow 0$  and extrapolated to the zero-range limit  $r_0 = 0$ . Instead, we optimize the ranges of the SGP. The two-body range  $r_0$  has been fixed to reproduce two data,  $E_2$  and  $r_B$  (or equivalently the effective range), in order to include finite-range corrections. The resulting two-body potential is of the same, next-to-leading, order that potentials with two derivatives [42]. Furthermore, fixing the three-body range  $\rho_0$  to optimize  $E_4$  we eventually reduce the residual effects of higher order forces. The final result is that these four observables,  $E_2$ ,  $r_B$ ,  $E_3$  and  $E_4$ , com-

	physical point		unitary point	
	SGP	HFD-HE2	SGP	HFD-HE2
$r_0[a_0]$	10.0485		10.0485	
$V_0[\text{K}]$	1.208018		1.150485	
$\rho_0[a_0]$	8.4853		8.4853	
$W_0[\text{K}]$	3.011702		3.014051	
$E_4[\text{K}]$	0.536	0.536	0.440	0.440
$E_5[\text{K}]$	1.251	1.266	1.076	1.076
$E_6[\text{K}]$	2.216	2.232	1.946	1.963
$E_{10}/10[\text{K}]$	0.792(2)	0.831(2)	0.714(2)	0.746(2)
$E_{20}/20[\text{K}]$	1.525(2)	1.627(2)	1.389(2)	1.491(2)
$E_{40}/40[\text{K}]$	2.374(2)	2.482(2)	2.170(2)	2.308(2)
$E_{70}/70[\text{K}]$	3.07(1)	3.14(1)	2.80(1)	2.92(1)
$E_{112}/112[\text{K}]$	3.58(2)	3.63(2)	3.30(2)	3.40(2)
$E_N/N(\infty)[\text{K}]$	7.2(3)*	7.14(2)	6.8(3)*	6.72(2)
HFD-B [K]		7.33(2)		6.73(2)

TABLE II. SGP parameters and the corresponding energies  $E_N$  or energies per particle  $E_N/N$  at the physical and unitary points. The values indicated with an asterisk (\*) are extrapolated results. The energies corresponding to the HFD-HE2 potential (in the last row the HFD-B potential) are given too.

pletely determine the SGP.

In the lower part of Table II the energy per particle is reported up to  $N = 112$ . The results for the infinite system are given in the last two rows where, the last one, includes the HFD-B saturation energy. We observe that the SGP energies follow the trend of those obtained with the realistic HFD-HE2 interaction which has a strong repulsive core. The weak repulsion in SGP introduced to describe correctly the trimer is sufficient to guarantee saturation of the system. With the selected value of  $\rho_0$ , the HFD-HE2 energies are reproduced for all  $N$  values within a 5% accuracy. An extrapolation to the infinite system, using a liquid drop formula, maintains the result within this limit (marked with an asterisk in the table). This is a remarkable result considering the minimal information included in the SGP.

We have discussed the property that different realistic He-He potentials give the same value of  $E_3$  and the same value of  $E_4$  when their strengths are reduced to locate them at unitarity. So, the four observables determining the SGP are independent of the potential used for its construction and, therefore, the saturation energy predicted by the SGP will be the same for all the He-He potentials. This suggests that all realistic He-He potentials should predict the same saturation energy at the unitary limit. To verify this prediction, we have calculated the saturation energy for the HFD-B model at the physical and unitary points reported in the last row of Table II. Although a difference is observed at the physical point, the latter is extremely close to the result of the HFD-HE2 potential confirming the collapse to a single value of the

saturation energy of the different He-He interactions at unitarity.

**Conclusions.** We have shown that the universal behavior observed in few-boson systems inside the unitary window can be characterized by paths constructed using gaussian potentials. For bosonic helium clusters this behaviour is well established up to  $N \approx 20$  and then smoothly deteriorates for larger  $N$  when short-range physics starts to play an explicit role introducing a non-universal behavior that competes with the universal characterization of the unitary window. Inside the universal regime the gaussian representation explains why, at unitarity, different He-He interactions give the same few-body binding energies.

To map the transition from universal to non-universal regime, we used the EFT framework, introducing a soft gaussian potential having a two-body plus a three-body term. Its parametrization, constrained from four data points, i.e. the scattering length, and the dimer, trimer and tetramer binding energies, resulted in a potential that predicted reasonably well the  $E_N/N$  ratio for all  $N$ , including the  $N \rightarrow \infty$  limit. To achieve this unexpected result we performed an optimization of the gaussian ranges,  $r_0$  and  $\rho_0$ , in order to reduce effects from higher order terms of the effective expansion that could appear in the description of more bound systems. In particular, the non-universal behavior introduced by the intrinsic repulsive short-range scale was mimicked by the properly chosen value of  $\rho_0$ . Importantly, our characterization can be readily explored in state-of-the-art experiments in ultracold quantum gases, where a fine control of the interaction strength is achieved allowing a detailed exploration of the unitary window. Finally, let us emphasize that our results should be independent of the gaussian form, other representations of the zero-range interaction can be used as well with the same conclusions [43].

**Acknowledgements.** B.J-D and A. P. acknowledge fruitful discussions with A. Sarsa. This work has been partially supported by MINECO (Spain) Grant No. FIS2017- 87534-P and from the European Union Regional Development Fund within the ERDF Operational Program of Catalunya (project QUASI-CAT/QuantumCat). N.K.T. acknowledges support from the United Kingdom Science and Technology Facilities Council (STFC) under Grant No. ST/L005743/1.

- 
- [1] V. Efimov, Phys. Lett. B **33**, 563 (1970).
  - [2] V. Efimov, Yad. Fiz. **12**, 1080 (1970) [Sov. J. Nucl. Phys. **12**, 589 (1971)].
  - [3] T. Kraemer *et al.*, Nature **440**, 315 (2006).
  - [4] M. Zaccanti *et al.*, Nat. Phys. **5**, 586 (2009).
  - [5] F. Ferlaino *et al.*, Few-Body Syst. **51**, 113 (2011).
  - [6] O. Matchey, Z. Shotan, N. Gross, and L. Khaykovich, Phys. Rev Lett. **108**, 210406 (2012).
  - [7] S. Roy *et al.*, Phys. Rev Lett. **111**, 053202 (2013).
  - [8] C. E. Klauss *et al.*, Phys. Rev Lett. **119**, 143401 (2017).
  - [9] E. Braaten and H.-W. Hammer, Phys. Rep. **428**, 259 (2006).
  - [10] P. Naidon and S. Endo, Rep. Prog. Phys. **80** 056001 (2017).
  - [11] H.W. Hammer and L. Platter, Eur. Phys. J. A **32**, 113 (2007).
  - [12] A. Deltuva, Phys. Rev. **A82**, 040701(R) (2010).
  - [13] J. von Stecher, J. D’Incao, and C. Greene, Nat. Phys. **5**, 417 (2009).
  - [14] A. Kievsky, N.K. Timofeyuk, and M. Gattobigio, Phys. Rev. **A90**, 032504 (2014).
  - [15] B. Bazak, M. Eliyahu, and U. van Kolck, Phys. Rev. **A94**, 052502 (2016).
  - [16] A. Kievsky and M. Gattobigio, Few-Body Syst. **57**, 217 (2016).
  - [17] S. König, H.W. Griesshammer, H.-W. Hammer, and U. van Kolck, Phys. Rev. Lett. **118**, 202501 (2017).
  - [18] M. Gattobigio, A. Kievsky and M. Viviani, Phys. Rev. **C100**, 034004 (2019).
  - [19] A. Kievsky and M. Gattobigio, Phys. Rev A **92**, 062715 (2015).
  - [20] R. Álvarez-Rodríguez, A. Deltuva, M. Gattobigio and A. Kievsky, Phys. Rev. A **93**, 062701 (2016).
  - [21] M. Gattobigio, M. Göbel, H.-W. Hammer and A. Kievsky, Few-Body Syst. **60**, 40 (2019).
  - [22] C. Chin, R. Grimm, P. Julienne, and E. Tiesinga, Rev. Mod. Phys. **82**, 1225 (2010).
  - [23] P.F. Bedaque, H.-W. Hammer, and U. van Kolck, Phys. Rev. Lett. **82**, 463 (1999).
  - [24] P. Bedaque, H.-W. Hammer, and U. van Kolck, Nucl. Phys. A **676**, 357 (2000).
  - [25] J. Carlson, S. Gandolfi, U. van Kolck, and S.A. Vitiello, Phys. Rev. Lett. **119**, 223002 (2017).
  - [26] R.E. Grisenti, W. Schöllkopf, J.P. Toennies, J.R. Manson, T.A. Savas, and Henry I. Smith, Phys. Rev. A **61**, 033608 (2000).
  - [27] M. Kunitski *et al.*, Science **348**, 551 (2015).
  - [28] E. Hiyama and M. Kamimura, Phys. Rev A **85**, 062505 (2012).
  - [29] R.A. Aziz, V.P.S. Nain, J.S. Carley, W.L. Taylor, and G.T. McConville, J. Chem. Phys. **70**, 4330 (1979).
  - [30] R.A. Aziz and M.J. Slaman, J. Chem. Phys. **94**, 8047 (1991).
  - [31] A.R. Jansen R.A. Aziz, J. Chem. Phys. **107**, 914 (1997).
  - [32] M. Jeziorska, W. Cencek, K. Patkowski, B. Jeziorski, and K. Szalewicz, J. Chem. Phys. **127**, 124303 (2007).
  - [33] W. Cencek, M. Przybytek, J.B. Mehl, J. Komasa, B. Jeziorski, and K. Szalewicz, J. Chem. Phys. **136**, 224303 (2012).
  - [34] R.A. Aziz, F.R.W. McCourt, and C.C.K. Wong, Mol. Chem. Phys. **61**, 1487 (1987).
  - [35] T. Korona, H.L. Williams, R. Bukowski, B. Jeziorski, and K. Szalewicz, J. Chem. Phys. **106**, 5109 (1997).
  - [36] E. Hiyama and M. Kamimura, Phys. Rev A **90**, 052514 (2014).
  - [37] N.K. Timofeyuk, Phys. Rev C **78**, 054314 (2008).
  - [38] N.K. Timofeyuk, Phys. Rev A **86**, 032507 (2012).
  - [39] A. Kievsky, A. Polls, B. Juliá Díaz, and N.K. Timofeyuk, Phys. Rev A **96**, 040501(R) (2017).
  - [40] P. Barletta and A. Kievsky, Phys. Rev. A **64**, 042514 (2001).

- [41] V. R. Pandharipande, J.G. Zabolitzky, S.C. Pieper, R.B. Wiringa, and U. Helmbrecht, Phys. Rev. Lett. **50**, 1676 (1983).
- [42] U. van Kolck, Nucl. Phys. **A645**, 273 (1999).
- [43] M. Gattobigio and A. Kievsky, Phys. Rev A **90**, 012502 (2014).